FORM FACTORS OF THE NEUTRON

H. SCHMIEDEN
Universität Mainz, Institut für Kernphysik, Mainz, Germany

Elastic form factors provide vital information about the charge and current distribution inside proton and neutron. Recent coincidence experiments improved our knowledge of the neutron form factors significantly. The results from the $^3\vec{H}e(\vec{e},e'n)$ and $D(\vec{e},e'\vec{n})$ double polarization experiments at MAMI indicate that the neutron electric form factor is almost a factor of two larger than previously assumed.

1 Introduction

The internal structure of the nucleon at very high energies is currently understood in terms of quarks and gluons, and described by perturbative QCD. However, at distances of the size of the nucleon and corresponding momentum transfers of about 1 GeV the strong coupling diverges. Therefore, perturbative methods completely fail to understand the variety of low energy phenomena of the nucleon, like anomalous magnetic moments, polarizabilities or radii. Despite first successes of lattice-QCD calculations [1] this is still a domain of models, which incorporate the basic symmetries of QCD in effective, multi-body degrees of freedom [2].

The elastic nucleon form factors parameterize the ability of the composite system to incorporate a momentum transfer, $\vec{q}$, coherently, i.e. without excitation and particle emission. They are related to the distribution of charge and currents and therefore of fundamental interest.

Since R. Hofstadter's pioneering experiments elastic electron scattering has become a unique tool for the investigation of the electromagnetic structure of the nucleon. In the simplest approximation, it is characterized by the exchange of one virtual photon, which transfers the momentum $\vec{q}$ and the energy ω. Electron scattering covers the spacelike region, because the squared four-momentum transfer, $q^2 = \omega^2 - \vec{q}^{\,2}$, is always negative. It is therefore usually expressed by the positive quantity $Q^2 = -q^2 > 0$. The timelike region, where $Q^2 < 0$, can be accessed through electron-positron annihilation into a pair of proton and anti-proton [3] or neutron and anti-neutron [4].

2 Nucleon form factors in elastic electron scattering

The charge-current density of the nucleon can be written in the form[5]:

$$\bar{N}\Gamma_\mu N = \bar{N}\left[\gamma_\mu F_1(Q^2) + \frac{i\sigma_{\mu\nu}q^\nu}{2m_N}\kappa F_2(Q^2)\right] N. \tag{1}$$

The *Dirac* form factor, $F_1(Q^2)$, modifies the vector current of charge and normal magnetic moment. Additionally, the *Pauli* form factor, $F_2(Q^2)$, parameterizes the effect of the anomalous magnetic moment, κ, as motivated by the Gordon decomposition of the electromagnetic current. Linear combinations of F_1 and F_2 constitute the electric and magnetic *Sachs* form factors[6]

$$G_E^{n,p}(Q^2) = F_1^{n,p}(Q^2) - \tau\kappa_{n,p}F_2^{n,p}(Q^2) \tag{2}$$
$$G_M^{n,p}(Q^2) = F_1^{n,p}(Q^2) + \kappa_{n,p}F_2^{n,p}(Q^2), \tag{3}$$

where $\tau = Q^2/4m_p^2$ is a dimensionless measure of the squared four-momentum transfer in units of the proton rest mass, m_p. These form factors correspond in the static limit, $Q^2 \to 0$, to the total charge and magnetic moment of protons and neutrons:

$$G_E^{n,p}(Q^2 \to 0) = 0,\ 1 \tag{4}$$
$$G_M^{n,p}(Q^2 \to 0) = -1.91,\, 2.79 \tag{5}$$

In the particular reference frame with vanishing energy transfer, the *Breit* frame, G_E and G_M can be interpreted as the Fourier transforms of the corresponding distributions of charge and magnetism, respectively. The interpretation of G_E in terms of the rest frame charge distribution is recently discussed again [7].

With these Sachs form factors the cross section for elastic electron-nucleon scattering can be written in the famous *Rosenbluth* form,

$$\frac{d\sigma}{d\Omega} = \left(\frac{d\sigma}{d\Omega}\right)_{\text{Mott}} \cdot \left(\frac{G_E^2 + \tau G_M^2}{1+\tau} + 2\tau G_M^2 \tan^2\frac{\vartheta_e}{2}\right), \tag{6}$$

where $\left(\frac{d\sigma}{d\Omega}\right)_{\text{Mott}}$ is the Mott cross section for electron scattering off a pointlike spin-$\frac{1}{2}$ object and ϑ_e denotes the electron scattering angle. Due to their different angular weights in Eq.6, G_E and G_M can be experimentally separated at constant Q^2.

This method of Rosenbluth-separation has been used in elastic electron-proton scattering [8,9] to determine G_E^p and G_M^p up to $Q^2 \simeq 9\,(\text{GeV/c})^2$. At higher Q^2 up to $30\,(\text{GeV/c})^2$, G_M^n dominates the cross section and has thus been determined directly [10]. The result is that G_E^p approximately follows the so-called dipole form,

$$G_E^p \simeq G_D = \left(1 + \frac{Q^2}{0.71\,(\mathrm{GeV/c})^2}\right)^{-2} \qquad \text{and}$$
$$G_M^p \simeq \mu_p G_D \tag{7}$$

scales with its magnetic moment. However, recent preliminary results[11] from measurements of the ratio of G_E^p/G_M^p in double polarized elastic scattering, $p(\vec{e}, e'\vec{p})$, seem to confirm the substantial deviation from the scaling behaviour at $Q^2 \geq 1.5$ (GeV/c)^2, which had already been indicated by older low statistics measurements[12,13].

Generally, the measurement of the neutron form factors raises more difficulties, because there is no free neutron target available which is suited for electron scattering experiments. The best possible approximation of free electron-neutron scattering is quasifree scattering off the lightest nuclei, usually the deuteron. In single arm experiments the dominating proton contribution has to be subtracted, with corresponding large uncertainties[14]. A Rosenbluth-separation has nevertheless been achieved [15] up to $Q^2 = 4\,(\mathrm{GeV/c})^2$. The neutron magnetic form factor exhibits the scaling behaviour, too,

$$G_M^n \simeq \mu_n G_D\,. \tag{8}$$

Coincidence experiments allow the explicit tagging of electron-neutron scattering [13,16,17,18,19]. The influence of binding effects can be minimized through the simultaneous measurement of the $D(e, e'p)$ reaction.

The situation concerning the neutron electric form factor, G_E^n, is most unfavourable. Due to the zero charge of the neutron it must vanish in the static limit

$$G_E^n(Q^2 \to 0) = 0. \tag{9}$$

The smallness of $(G_E^n)^2$ compared to $\tau(G_M^n)^2$ makes a Rosenbluth decomposition (Eq.6) very difficult. Due to the corresponding large errors in the small quantity the extracted values for G_E^n are compatible with zero[13,15]. Therefore, in the momentum transfer range $Q^2 < 1\,(\mathrm{GeV/c})^2$ the most precise data came from *elastic* electron-deuteron scattering[20,21], where the structure function $A(Q^2)$ depends on the isoscalar form factor $(G_E^p + G_E^n)^2$ and thus provides a higher sensitivity to G_E^n through its interference with the large G_E^p. However, the necessary unfolding of the deuteron wavefunction introduces a substantial model dependence in the extracted neutron electric form factor.

3 G_M^n coincidence experiments

Though in principle also accessible in inclusive quasielastic scattering of longitudinally polarized electrons off polarized $^3\vec{He}$ [22], the most precise recent determinations of G_M^n come from unpolarized coincidence experiments at Bates[16], NIKHEF[17], ELSA[18], and MAMI[19]. Except the Bates experiment, which measured the absolute $D(e,e'n)$ cross section, these experiments determine G_M^n from the ratio $R = \frac{\sigma(e,e'n)}{\sigma(e,e'p)}$ of quasifree neutron over proton cross sections off the deuteron with simultaneous neutron/proton detection in one single hadron detector. This ratio method is independent of nuclear binding effects, which cancel to a large extent, and also experimentally insensitive to

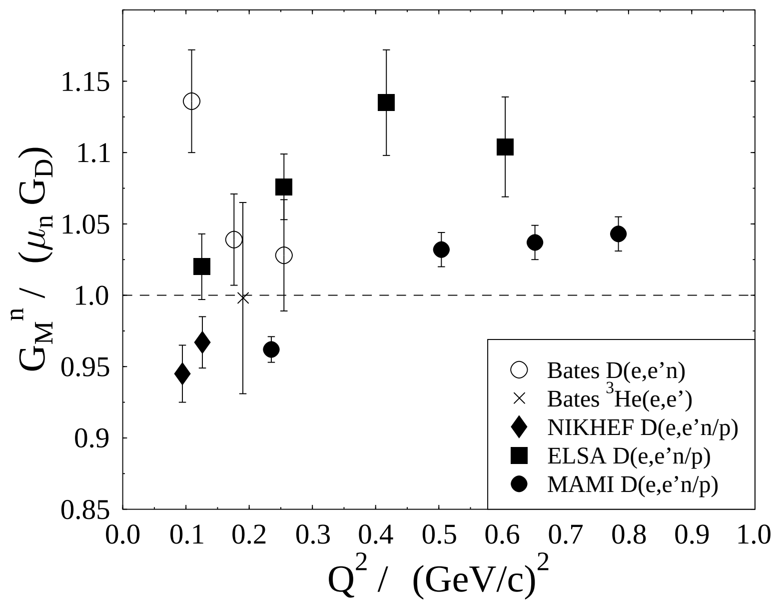

Figure 1. Results of recent G_M^n experiments. Gao et al.[22] exploited the $^3\vec{He}(\vec{e},e')$ cross section asymmetry (cross). The open circles are the result of the D$(e,e'n)$ experiment of Markowitz et al.[16]. Bruins et al.[18] (full squares) and Anklin et al. (diamonds[17] and full circles[19]) made use of the ratio method as described in the text.

luminosity fluctuations and detector acceptancies.

Nevertheless, detailed control of the hadron detector's absolute detection efficiency for protons and, particularly, neutrons is essential. The setups of the experiments have been very similar with the electron detected in a magnetic spectrometer and coincident n/p-detection in a well shielded plastic or mineral oil scintillator telescope. However, different approaches have been used to determine the absolute neutron detection efficiency. For the Bates and ELSA measurements "in situ" methods were chosen with a bremsstrahlung radiator postioned in front of the experimental target in order to exploit the $D(\gamma,p)n$ or $p(\gamma,\pi^+)$ reactions, respectively, to tag neutrons in the telescope. The possible impact of un-tagged electroproduction events is currently under discussion[23,24]. In contrast, the hadron detectors which were used at MAMI and NIKHEF were calibrated at the PSI neutron beam in a kinematically complete $p(n,p)n$ experiment. This method relies on the good control and portability of the effective detector thresholds.

Figure 1 shows a comparison of the recent results from Bates[16,22], ELSA[18], NIKHEF[17], and MAMI[19]. Despite the individual errors of down to 2 %, the MAMI data are approximatly 10 - 15 % below the ELSA ones. This stresses the importance of the absolute neutron detection efficiency calibration, which appears to be the probable origin of this discrepancy.

4 G_E^n double polarization experiments

Double polarization observables in quasifree electron-deuteron scattering with longitudinally polarized electrons offer high sensitivity to G_E^n, due to an interference with the large G_M^n, combined with negligible dependence on the deuteron wavefunction [25]. For the ideal case of free electron-neutron scattering, $n(\vec{e},e'\vec{n})$, Arnold, Carlson and Gross [26] obtained for the components of the recoil polarization

$$P_x = -P_e \frac{\sqrt{2\tau\epsilon(1-\epsilon)}G_E^n G_M^n}{\epsilon(G_E^n)^2+\tau(G_M^n)^2} \tag{10}$$

$$P_y = 0 \tag{11}$$

$$P_z = P_e \frac{\tau\sqrt{1-\epsilon^2}(G_M^n)^2}{\epsilon(G_E^n)^2+\tau(G_M^n)^2}, \tag{12}$$

where $\hat{x}$ is in the electron scattering plane perpendicular to the direction of the momentum transfer, $\hat{y}$ is normal to the scattering plane, and $\hat{z}$ points into the direction of the momentum transfer, $\vec{q}$ (compare Fig.2). $\epsilon = (1+\frac{2|\vec{q}|^2}{Q^2}\tan^2\frac{\vartheta_e}{2})^{-1}$ is the photon polarization parameter and P_e denotes the longitudinal polarization of the electron beam.

In the completely equivalent scattering of longitudinally polarized electrons off a polarized neutron target, $(\vec{n}(\vec{e},e'n))$, the cross section asymmetry with regard to reversal of the electron beam polarization is given by

$$A = -P_e \frac{\sqrt{2\tau\epsilon(1-\epsilon)}G_E^n G_M^n \cdot \tilde{P}_x + \tau\sqrt{1-\epsilon^2}(G_M^n)^2 \cdot \tilde{P}_z}{\epsilon(G_E^n)^2 + \tau(G_M^n)^2}, \tag{13}$$

where now $\tilde{P}_{x,z}$ are the components of the initial state neutron polarization. The polarized target neutrons can be provided by polarized $^3\vec{\mathrm{He}}$ [27]. In the asymmetry ratio $\frac{A_x(\tilde{P}_z=0)}{A_z(\tilde{P}_x=0)}$ the absolute degree of the target polarization cancels out [28,29].

4.1 The $D(\vec{e},e'\vec{n})$ experiment at MAMI

The longitudinally polarized electron beam ($I \simeq 2.5\,\mu$A, $P_e \simeq 75\,\%$) hit a 5 cm long liquid hydrogen target and the scattered electrons were detected in a 256 element lead glass array, which covered a solid angle of $\Delta\Omega \simeq 100$ msr (Fig.3). The energy resolution of $\delta E/E \simeq 25\,\%$ was sufficient to suppress pion production events. Only the electron angles, which were measured with an accuracy of $\delta\vartheta, \delta\phi \simeq 3.5$ mrad entered the event reconstruction, which became kinematically complete through the measurement of the neutrons time-of-flight and hit position in the front plane of the neutron detector.

The neutron polarization can be analyzed in the detection process itself[30]. This required a second neutron detection in one of the rear detector planes,

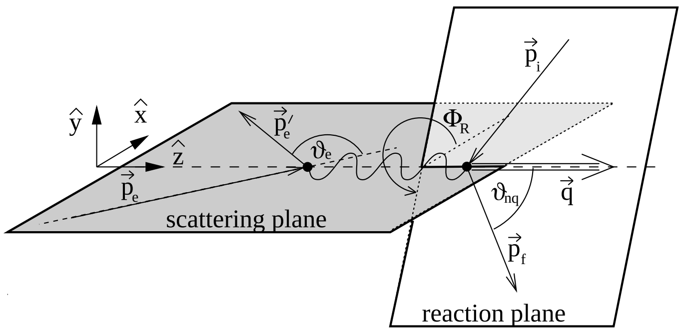

Figure 2. Kinematics of the quasifree $n(\vec{e},e'\vec{n})$ reaction with definition of the relevant coordinate frames.

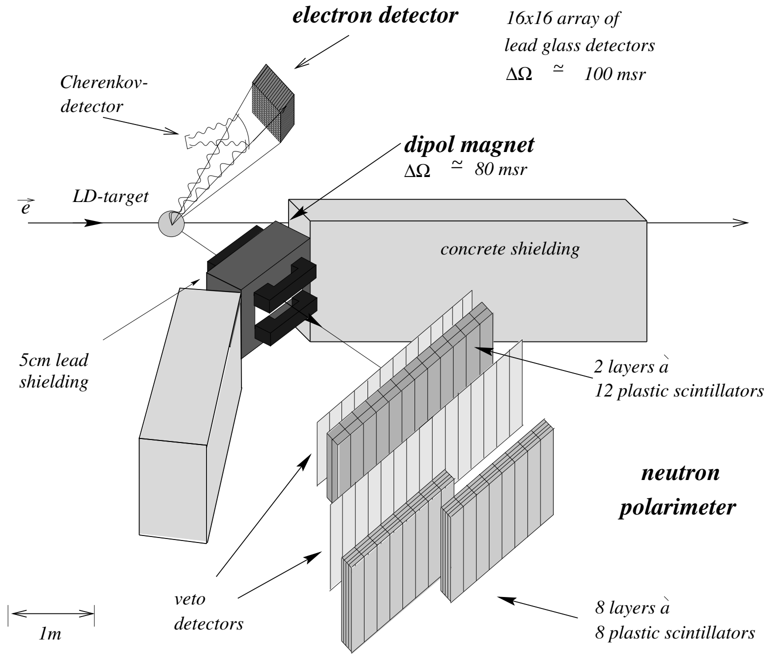

Figure 3. Setup of the $D(\vec{e}, e'\vec{n})$ experiment at MAMI

which yielded the polar and azimuthal angles, Θ_n' and Φ_n', of the analyzing scattering in the front wall. With the number of events $N^{\pm}(\Phi_n')$ for $\pm$ helicity states of the electron beam the azimuthal asymmetry, $A(\Phi_n')$, was determined through the ratio

$$\frac{1 - A(\Phi_n')}{1 + A(\Phi_n')} = \sqrt{\frac{N^+(\Phi_n') \cdot N^-(\Phi_n' + \pi)}{N^-(\Phi_n') \cdot N^+(\Phi_n' + \pi)}}, \tag{14}$$

which is insensitive to detector efficiencies and luminosity variations. The extraction of P_x from $A(\Phi_n') = \epsilon_{\text{eff}} \cdot P_x \cdot \sin \Phi_n'$ requires the calibration of the effective analyzing power, ϵ_{eff}, of the polarimeter. This, however, varies strongly with the event composition as determined by hardware conditions during data taking and software cuts applied in the offline analysis.

For the first time, the problem of calibration of the effective analyzing power has been avoided by controlled precession of the neutron spins in the field of a dipole magnet in front of the polarimeter [31] (see Fig.3). After precession by the angle χ the transverse neutron polarization behind the magnet, $P_\perp$, is a superposition of x and z components, and likewise is the measured asymmetry:

$$A_\perp = A_x \cos\chi - A_z \sin\chi. \tag{15}$$

In the particular case of the zero crossing, $A_\perp(\chi_0) = 0$, one immediately gets the relation

$$\tan\chi_0 = \frac{A_x}{A_z} = \frac{\epsilon_{\text{eff}} \cdot P_e \cdot \sqrt{2\tau\epsilon(1-\epsilon)}\, G_E^n \cdot G_M^n}{\epsilon_{\text{eff}} \cdot P_e \cdot \tau\sqrt{1-\epsilon^2}\,(G_M^n)^2}. \tag{16}$$

Obviously, this ratio is independent of both the degree of electron beam polarization, P_e, and the polarimeter's effective analyzing power. It therefore directly yields G_E^n/G_M^n. Different effective analyzing powers do change the magnitude of the transverse asymmetry, $A_\perp$, but not the zero crossing angle, χ_0[31].

4.2 Final state interaction

Data have been taken around $Q^2 = 0.32\,(\text{GeV/c})^2$ and $Q^2 = 0.12\,(\text{GeV/c})^2$. According to calculations of H. Arenhövel [32] the effect of final state interaction on P_x – which is dominated by charge exchange of the outgoing nucleons – is almost negligible at the higher momentum transfer. However, due to the small relative energy in the n-p final state, it becomes important at the small Q^2. This is illustrated in Fig.4. P_x, as calculated for the event population of the present experiment[33], is plotted as a function of the angle ϑ_{nq} of the outgoing neutron with respect to $\vec{q}$ for the two extreme situations $\Phi_R = 0$ (left of $\vec{q}$) and $\Phi_R = 180^o$ (right of $\vec{q}$). For $\vartheta_{nq} \leq 10^o$ the general behaviour is well approximated by purely kinematical effects due to fermi motion and can therefore be understood within a kinematical model[33] (dashed-dotted curves). The effect of final state interaction is exhibited in the difference between the dashed lines (Born calculation, i.e. without FSI) and the full curves, which include FSI. As expected, this difference is very small at $Q^2 = 0.32\,(\text{GeV/c})^2$ (Fig.4, left), but it is roughly 50 % at $Q^2 = 0.12\,(\text{GeV/c})^2$ (Fig.4, right). Despite its size, the required correction of the G_E^n/G_M^n ratio extracted from P_x has only small uncertainties, because it is insensitive to the choice of N-N potential and G_E^n parameterization [32]. Therefore, even at $Q^2 = 0.12\,(\text{GeV/c})^2$ a reliable extraction of G_E^n/G_M^n is possible. The longitudinal neutron polarization, P_z, remains almost unaffected by FSI.

The neutron electric form factor, G_E^n, has been extracted from the ratio G_E^n/G_M^n relying on the dipole values for G_M^n (Eq.8). In order to account for

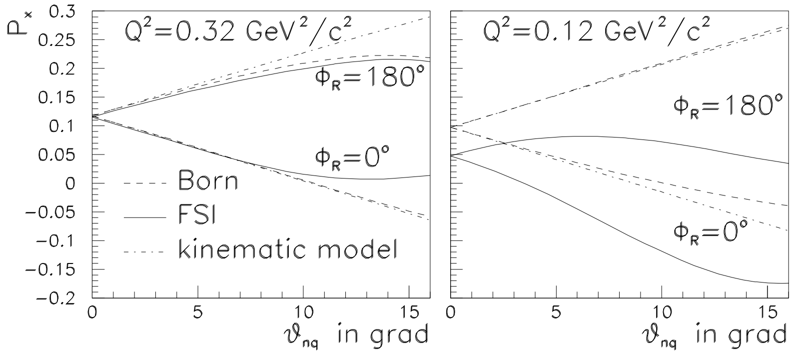

Figure 4. The polarization component P_x, calculated for the event population of the $D(\vec{e},e'\vec{n})$ experiment at MAMI, as a function of the angle between the outgoing neutron and the momentum transfer direction, ϑ_{np}, without final state interaction (Born) and with final state interaction (FSI). Left and right parts are for $Q^2 = 0.32\,(\mathrm{GeV/c})^2$ and $Q^2 = 0.12\,(\mathrm{GeV/c})^2$, respectively. The kinematical model takes into account only the proper rotation of quantization axes between neutron rest frame and laboratory frame required by fermi motion.

the present experimental discrepancy in G_M^n, an additional 5 % systematic error has been assigned. The results are depicted in Fig.5 as full circles with statistical (inner) and systematical (outer) error. So far, only for the MAMI $D(\vec{e},e'\vec{n})$ data a FSI correction has been applied. In view of the size of the errors such a correction seems unnecessary for the Bates $D(\vec{e},e'\vec{n})$ data point[34] (open circle). The full squares represent the MAMI results for $^3\vec{H}e(\vec{e},e'n)$. At $Q^2 = 0.6\,(\mathrm{GeV/c})^2$ [29] FSI is expected to be negligible due to the large kinetic energy of the ejected neutron. However, first, still incomplete 3-body calculations [35] indicate a substantial correction of the data point at $Q^2 = 0.36\,(\mathrm{GeV/c})^2$ (full square)[36] towards larger G_E^n. Excluding this data point, a new one parameter fit to the recent MAMI double polarization results yielded

$$G_E^n = -\frac{\mu_n \tau}{1+\eta\tau} \cdot G_D \tag{17}$$

with $\eta = 3.4$. Such a fit reproduces within the errors the neutron's measured rms charge radius[37], which is related to the slope of $G_E^n(Q^2 \to 0)$ as indicated in Fig.5. It lies almost a factor of two above the so far favoured result, G_P, from elastic $D(e,e')$ scattering, where the Paris potential has been used for the unfolding of the wave function contribution[21].

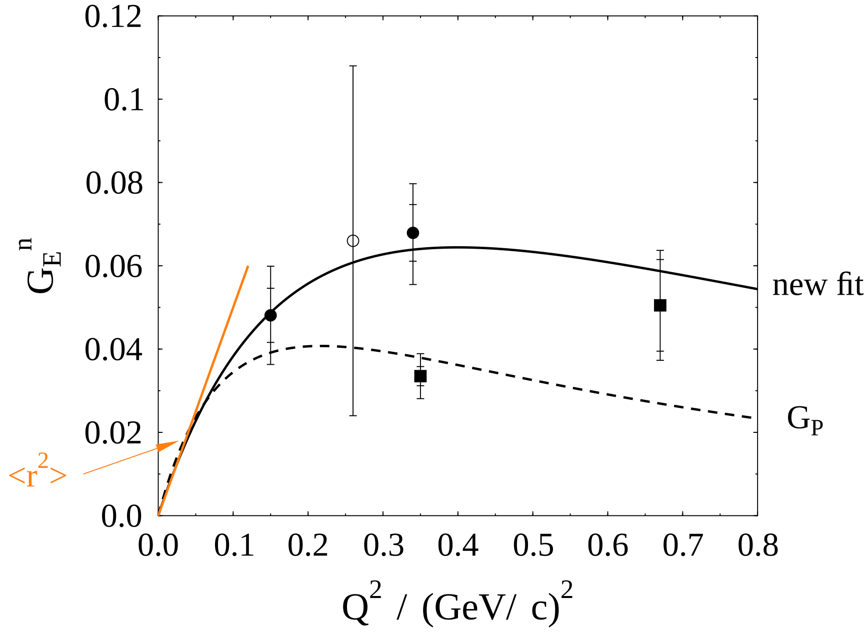

Figure 5. Results for G_E^n from the $D(\vec{e}, e'\vec{n})$ experiment at MAMI (full circles)[31,33] along with the $^3\vec{H}e(\vec{e}, e'n)$ results from MAMI (full squares)[29,36] and $D(\vec{e}, e'\vec{n})$ results from Bates (open circle)[34]. The curves are discussed in the text.

5 Summary

Elastic form factors contain information about the distribution of charge and current in the nucleon ground state. Precise proton data are available up to $Q^2 = 30$ (GeV/c)^2. The neutron magnetic form factor, G_M^n, could be extracted up to $Q^2 = 4$ (GeV/c)^2 from single arm $D(e, e')$ quasielastic scattering. Below $Q^2 = 1$ (GeV/c)^2, recent coincidence experiments allowed a precise determination of G_M^n from the ratio $R = \frac{\sigma(e,e'n)}{\sigma(e,e'p)}$ of quasifree electron scattering cross sections off the deuteron. Despite their individual statistical errors of only 2 %, the datasets from ELSA and MAMI differ by as much as 10

- 15 %. This discrepancy urgently needs clarification, also as a normalization for the recent double polarization experiments $^3\vec{H}e(\vec{e}, e'n)$ and $D(\vec{e}, e'\vec{n})$ at MAMI, which measure the ratio G_E^n/G_M^n of electric to magnetic neutron form factors. In the $D(\vec{e}, e'\vec{n})$ experiment the neutron polarimeter was, for the first time, supplemented by a spin precessing dipole magnet. This avoided the problem of its analyzing power calibration. The influence of final state interaction has been quantitatively evaluated for the $D(\vec{e}, e'\vec{n})$ reaction. At the lowest Q^2 a significant FSI correction is required for the extracted G_E^n. After this correction the data are consistently described by a new one parameter fit which lies almost a factor of two above the so far favoured result from elastic electron deuteron scattering.

6 Acknowledgements

The MAMI experiments have been performed within the framework of the collaborations A1 and A3 with contributions of institutes of the universities of Basel, Bonn, Glasgow, Mainz, and Tübingen. H. Arenhövel supplied us with all the necessary calculations for the FSI correction. The spin precession magnet for the $D(\vec{e}, e'\vec{n})$ experiment was provided by the Physikalisches Institut of the university of Bonn. Financial support came from the Deutsche Forschungsgemeinschaft (SFB 201).

References

1. S.J. Dong et al., *Phys. Rev.* D **58**, 074504 (1997) and references therein
2. see for example: R. Bijker and A. Leviatan, contributed paper to this conference; D.H. Lu et al., *Phys. Rev.* C **57**, 2628 (1997) and references therein
3. T.A. Armstrong et al., *Phys. Rev. Lett.* **70**, 1212 (1993), and G. Bardin et al., *Nucl. Phys.* B **411**, 3 (1994) and references therein
4. A. Antonelli et al., *Nucl. Phys.* B **517**, 3 (1998), see also R. Baldini, contributed paper to this conference
5. J.D. Bjørken and S.D. Drell, Relativistic quantum mechanics, McGraw-Hill 1964
6. R.G. Sachs, *Phys. Rev.* **126**, 2256 (1962)
7. N. Isgur, hep-ph/9812243
8. P. Bosted et al., *Phys. Rev. Lett.* **68**, 3841 (1992)
9. A.F. Sill et al., *Phys. Rev.* D **48**, 29 (1993)
10. R.G. Arnold et al., *Phys. Rev. Lett.* **57**, 174 (1986)

11. G. Quéméner et al., Proceedings of the Int. Nucl. Physics Conference, INPC, Paris 1998
12. Ch. Berger et al., *Phys. Lett.* B **35**, 87 (1971)
13. W. Bartel et al., *Nucl. Phys.* B **58**, 429 (1973)
14. for a compilation see I. Sick, Proc. 6^{th} Miniconference on electron scattering, p. 193, NIKHEF 1989
15. A. Lung et al., *Phys. Rev. Lett.* **70**, 718 (1993)
16. P. Markowitz et al., *Phys. Rev.* C **48**, R5 (1993)
17. H. Anklin et al., *Phys. Lett.* B **336**, 313 (1994)
18. E. Bruins et al., *Phys. Rev. Lett.* **75**, 21 (1995)
19. H. Anklin et al., *Phys. Lett.* B **428**, 248 (1998)
20. S. Galster et al., *Nucl. Phys.* B **32**, 221 (1971)
21. S. Platchkov et al., *Nucl. Phys.* A **510**, 740 (1990)
22. H. Gao et al., *Phys. Rev.* C **50**, R546 (1994)
23. J. Jourdan et al., *Phys. Rev. Lett.* **79**, 5186 (1997)
24. E. Bruins et al., *Phys. Rev. Lett.* **79**, 5187 (1997)
25. H. Arenhövel, *Phys. Lett.* B **199**, 13 (1987) and *Z. Phys.* A **331**, 509 (1988)
26. R.G. Arnold et al., *Phys. Rev.* C **23**, 363 (1981)
27. G. Eckert et al., *Nucl. Instrum. Methods* A **320**, 53 (1992) and W. Heil et al., *Phys. Lett.* A **201**, 337 (1995)
28. P. Grabmayr, contributed paper to this conference
29. D. Rohe, doctoral thesis, Mainz 1998, and proceedings of the 'Workshop on polarized targets and beams', Champaign/Illinois 1997
30. T.N. Taddeucci et al., *Nucl. Instrum. Methods* A **241**, 448 (1985)
31. M. Ostrick et al., submitted to *Phys. Rev. Lett.*
32. H. Arenhövel, priv. comm., 1998
33. C. Herberg, doctoral thesis, Mainz 1998
34. T. Eden et al., *Phys. Rev.* C **50**, R1749 (1994)
35. W. Glöckle, priv. comm., and G. Ziemer, doctoral thesis, Bochum (in preparation)
36. J. Becker, doctoral thesis, Mainz 1997
37. S. Kopecki et al., *Phys. Rev.* C **56**, 2229 (1997)